www.coinweb.no

SINTEF Building and Infrastructure Tore Myrland Jensen and Jan Arve Øverli

Experimental study on flexural ductility in over-reinforced light-weight aggregate concrete beams

COIN Project report 70 – 2015

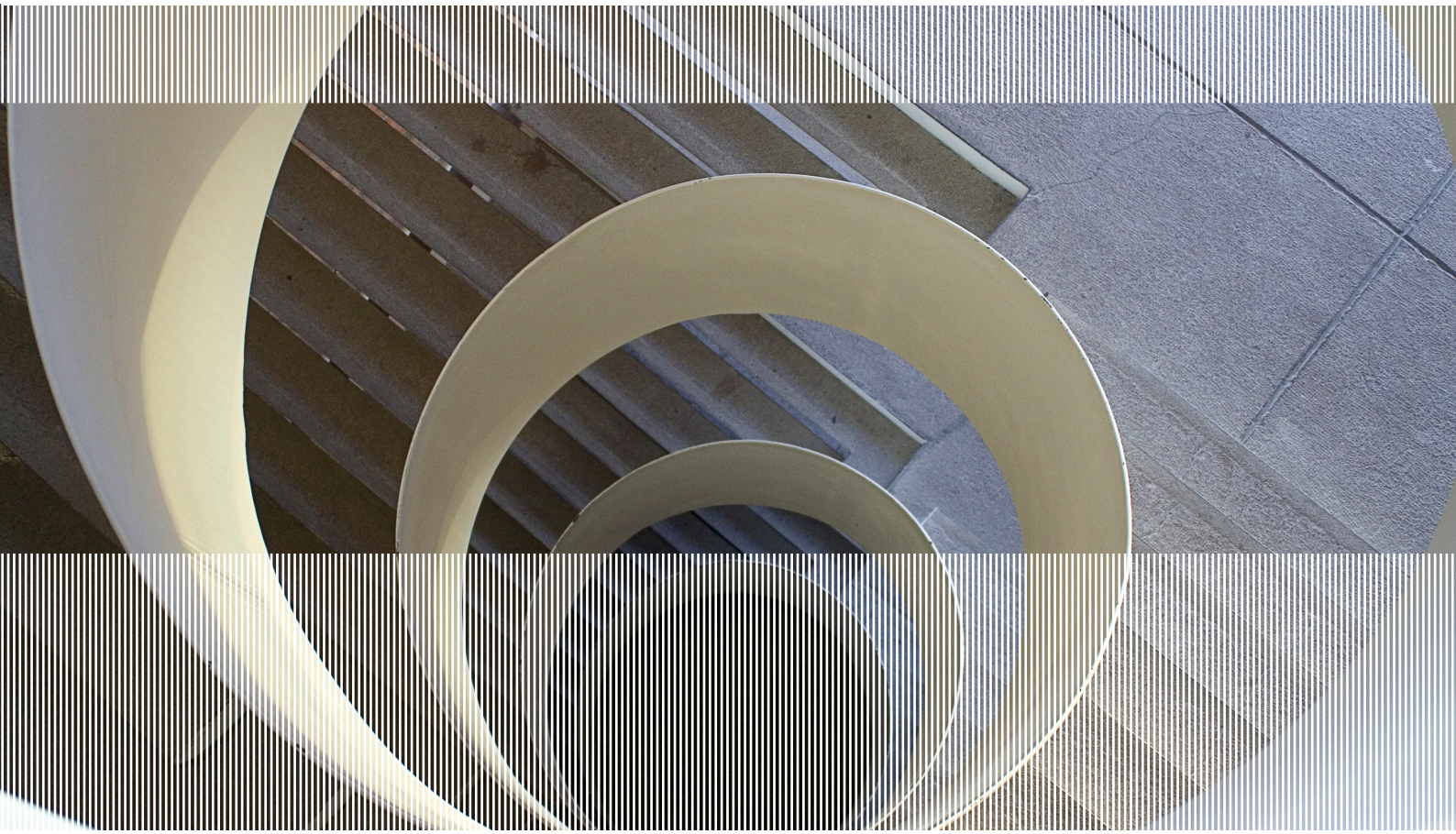

SINTEF

SINTEF Building and Infrastructure

Tore Myrland Jensen and Jan Arve Øverli

Experimental study on flexural ductility in over-reinforced lightweight aggregate concrete beams

FA 3 Aesthetics and technical performance

SP 3.3 Structural Performance

COIN Project report 70 – 2015

COIN Project report no 70
Tore Myrland Jensen and Jan Arve Øverli
Experimental study on flexural ductility in over-reinforced lightweight aggregate concrete beams
FA 3 Aesthetics and technical performance
SP 3.3 Structural Performance

Keywords:
Lightweight concrete, Confinement, Ductility, Steel fibre, Steel transverse reinforcement, Bending tests

Project no.: 102000442-8

Photo, cover: «Spiral», iStock

ISSN 1891–1978 (online)
ISBN 978-82-536-1470-0 (pdf)

Address: Forskningsveien 3 B
POBox 124 Blindern
N-0314 OSLO
Tel: +47 22 96 55 55
Fax: +47 22 69 94 38 and 22 96 55 08

www.sintef.no/byggforsk
www.coinweb.no

Cooperation partners / Consortium Concrete Innovation Centre (COIN)

Kværner Engineering
Contact: Jan-Diederik Advocaat
Email: Jan-Diederik.Advocaat@kvaerner.com
Tel: +47 67595050

Saint Gobain Weber
Contact: Geir Norden
Email: geir.norden@saint-gobain.com
Tel: +47 22887700

Norcem AS
Contact: Terje Rønning
Email: terje.ronning@norcem.no
Tel: +47 35572000

NTNU
Contact: Terje Kanstad
Email: terje.kanstad@ntnu.no
Tel: +47 73594700

Mapei AS
Contact: Trond Hagerud
Email: trond.hagerud@mapei.no
Tel: +47 69972000

SINTEF Building and Infrastructure
Contact: Tor Arne Hammer
Email: tor.hammer@sintef.no
Tel: +47 73596856

Skanska Norge AS
Contact: Sverre Smeplass
Email: sverre.smeplass@skanska.no
Tel: +47 40013660

Norwegian Public Roads Administration
Contact: Kjersti K. Dunham
Email: kjersti.kvalheim.dunham@vegvesen.no
Tel: +47 22073940

Unicon AS
Contact: Stein Tosterud
Email: stto@unicon.no
Tel: +47 22309035

Veidekke Entreprenør ASA
Contact: Christine Hauck
Email: christine.hauck@veidekke.no
Tel: +47 21055000

Preface

This study has been carried out within COIN - Concrete Innovation Centre - one of presently 14 Centres for Research based Innovation (CRI), which is an initiative by the Research Council of Norway. The main objective for the CRIs is to enhance the capability of the business sector to innovate by focusing on long-term research based on forging close alliances between research-intensive enterprises and prominent research groups.

The vision of COIN is creation of more attractive concrete buildings and constructions. Attractiveness implies aesthetics, functionality, sustainability, energy efficiency, indoor climate, industrialized construction, improved work environment, and cost efficiency during the whole service life. The primary goal is to fulfil this vision by bringing the development a major leap forward by more fundamental understanding of the mechanisms in order to develop advanced materials, efficient construction techniques and new design concepts combined with more environmentally friendly material production.

The corporate partners are leading multinational companies in the cement and building industry and the aim of COIN is to increase their value creation and strengthen their research activities in Norway. Our over-all ambition is to establish COIN as the display window for concrete innovation in Europe.

About 25 researchers from SINTEF (host), the Norwegian University of Science and Technology - NTNU (research partner) and industry partners, 15 - 20 PhD-students, 5 - 10 MSc-students every year and a number of international guest researchers, work on presently eight projects in three focus areas:

- Environmentally friendly concrete
- Economically competitive construction
- Aesthetic and technical performance

COIN has presently a budget of NOK 200 mill over 8 years (from 2007), and is financed by the Research Council of Norway (approx. 40 %), industrial partners (approx 45 %) and by SINTEF Building and Infrastructure and NTNU (in all approx 15 %).

For more information, see www.coinweb.no

Tor Arne Martius-Hammer
Centre Manager

Summary

This study focuses on ductility of lightweight aggregate concrete (LWAC) in compression. The major disadvantage of LWAC is the brittleness in compression at the material level compared to normal density concrete. Requirements for energy absorption and/or a controlled behaviour after peak load may exclude LWAC as the preferred material. In overload situations adequate ductility is essential to ensure safety. Floating offshore structures and LNG-terminals are often post-tensioned, e.g. to avoid leakage cracks in service. Thus the compressive ductility is of great importance. The influence of the stress-strain characteristics in compression is also more pronounced in structures subjected to combined bending moment and axial forces. Ductility of LWAC in compression plays an important part in improving the structural ductility in heavily reinforced and post-tensioned structures. Increase of the ductility in the compression zone in bending is possible by employing stirrups and/or fibre reinforcement to achieve passive confinement.

To study the ductility an experimental program was set up consisting of eight over-reinforced light-weight concrete beams with length 4200 mm and cross-section 400×350 mm, which were subjected to four-point bending. The beams were heavily over-reinforced to ensure spalling in the compression zone of the cross section before yielding of the tensile reinforcement. The LWAC had a mass density about 1800 kg/m^3, with a compressive strength about 35 MPa. Four different confinement configurations of the compression zone of the beams were investigated - only LWAC, 1 % of steel fibre reinforcement, stirrups with spacing 100 mm, and a combination of fibre and stirrups. This report presents mainly the results from the experimental investigation of the beams, with focus on the flexural response. Especially the effect of the different confinement configurations is analysed in the plastic hinge region. However, also the obtained material properties of the LWAC, the fibre reinforced LWAC and the reinforcement are given. In addition the governing design assumptions employed for calculated load capacities are illustrated, and also the estimation of the displacement-, rotation- and curvature relationships.

The load at spalling of the concrete cover and the pre-peak response before initiation of spalling was approximately the same for all configurations. However, the effects of the different confinement configurations on the post-peak response are significant within the inelastic range of deformations, i.e. considerable improvement of the structural performance regarding ductility and load-carrying degradation. As expected, the reference beams with only LWAC in the compression zone, had a brittle post-peak response, i.e. no post-peak deformability and a very steep descending branch immediately after initiation of spalling of the concrete cover. The other beams, with different confinement configurations, were all capable of carrying load with quite large deflections, and also achieved a peak load after initiation of spalling.

Beams with fibre had a soft transition at spalling, with a steady flattening of the load-deformation relationship, before the peak load was achieved. Beams with stirrups show a reduced capacity after initiation of spalling, before the confinement effect of the stirrups was activated and the load capacity was increasing again towards the peak load. For these beams, with either fibre or stirrups in the compression zone, the peak load was achieved at a load approximately equal to the load at spalling, and with a displacement ductility index ($\mu_2 = \Delta_{peak}/\Delta_{spall}$) of about 1,2. Beams with both fibre and stirrups had a soft transition at spalling, but also a gradual and significant capacity increase of approximately 10 % after initiation of spalling, and achieved a displacement ductility index ($\mu_2 = \Delta_{peak}/\Delta_{spall}$) of about 1,5.

Beams with either fibre or stirrups experienced approximately the same post-peak response. However, the two beams with fibre had a large difference in the inclination of the descending branch after peak load. This can partly be explained by different fibre distribution and fibre orientation. For these beams the achieved displacement ductility index ($\mu_3 = \Delta_{0,9spall}/\Delta_{spall}$), referred to as the ratio of the vertical mid span displacement at 90 % of the spalling load in the post-peak response to the displacement at spalling load, was about 1,8. Beams with both fibre and stirrups had a very ductile post-peak response, with a slight descending branch, and achieved a displacement ductility index ($\mu_3 = \Delta_{0,9spall}/\Delta_{spall}$) of about 4,0, i.e. approximately doubled compared to the beams with either fibre or stirrups. Thus, the effect of using both fibres and stirrups was advantageous and significant with respect to ductility in the post-peak response, in addition to the ultimate capacity.

The results from this investigation are promising, and indicate that LWAC have potential to be consistent with the performance requirements for structural materials, also regarding ductility in heavily reinforced and post-tensioned structures in seismic areas.

Keywords: Bending tests, Confinement, Ductility, Lightweight concrete, Steel fibre, Stirrups

Table of contents

NOTATIONS **6**

1 INTRODUCTION **8**

2 EXPERIMENTAL PROGRAM **10**

2.1 OVERVIEW – BEAM DESIGN 10
2.2 MATERIALS AND MIX PROPORTIONS 12
2.3 MECHANICAL PROPERTIES 13
2.3.1 Properties in compression, LWAC 13
2.3.2 Residual flexural tensile strength, FRLWAC 17
2.3.3 Reinforcement 18
2.4 INSTRUMENTATION AND TEST PROCEDURE 19

3 TEST RESULTS AND DISCUSSION **21**

3.1 MAIN RESULTS 21
3.2 LOAD-DISPLACEMENT RELATIONSHIPS 22
3.3 CONCRETE AND STEEL STRAINS 26
3.3.1 Strain curves 26
3.3.2 Strain distribution in cross-section at peak-loads 27
3.4 FAILURE MODE AND ULTIMATE STRENGTH 29

4 DUCTILITY **34**

4.1 OVERVIEW 34
4.2 DUCTILITY CHARACTERISTICS 35
4.3 DISPLACEMENT RELATIONSHIPS WITHIN THE PLASTIC HINGE REGION 37
4.4 DISPLACEMENT-, ROTATION- AND CURVATURE RELATIONSHIPS 41

5 CONCLUSION **43**

6 ACKNOWLEDGEMENTS **45**

REFERENCES **46**

APPENDICES **48**

APPENDIX A1: LOAD CURVES 48
APPENDIX A2: STRAIN CURVES 50
APPENDIX A3: TRANSVERSAL STRAIN DISTRIBUTION 52
APPENDIX A4: CALCULATION MODEL FOR P_{SPALL} AND P_{PEAK} 53
APPENDIX A5: DISPLACEMENT-, ROTATION- AND CURVATURE RELATIONSHIPS 56
APPENDIX A6: COMPRESSIVE STRENGTH AND DENSITY – LWAC 57
APPENDIX A7: NUMBER OF FIBRES IN SMALL SCALE BEAMS 58

Notations

The most commonly used notations and their meaning are listed below. Other notations and symbols are explained in the text when they first appear.

Latin letters

a	shear span of the beam
b	with of the beam
d	effective beam depth
d_r	reduced effective beam depth after spalling
f_{lc}	compressive strength of light weight aggregate concrete
$f_{lc,c}$	compressive strength of confined light weight aggregate concrete
f_{lcm}	mean value of light weight concrete compressive cylinder strength
f_y	yield strength of reinforcement
h	beam depth
h_r	reduced effective beam depth after spalling
t	time [minute]
t_0	the age at the time of loading [days]
z	lever arm of internal forces
A	cross-sectional area
A_s	cross-sectional area, tensile reinforcement
A_s'	cross-sectional area, compression reinforcement
A_{st}	cross-sectional area, transversal reinforcement
E	modulus of elasticity
E_{lc}	modulus of elasticity for LWAC in compression
E_s	modulus of elasticity for reinforcement
L	length
L^p	length of plastic hinge
M	bending moment
M_{spall}	moment at spalling of concrete in compression
M_{peak}	moment at max load after spalling
P	load
P_{spall}	load at spalling of concrete in compression (first peak load)
P_{peak}	max load at top of ascending branch after spalling (second peak load)
$P_{0,9spall}$	load in the post-peak response (90 % of the load at spalling, P_{spall})
P_c	internal compressive force LWAC
P_r	internal compressive force reinforcement
S	internal tensile force reinforcement
S_t	internal tensile force in transversal reinforcement
W	energy absorption
W_{el}	elastic energy absorption
W_{in}	inelastic energy absorption

Greek letters

Δ	displacement
Δ_c	elastic mid span displacement at max load
Δ_{spall}	mid span displacement at load at spalling, P_{spall}
Δ_{peak}	mid span displacement at peak load, P_{peak}
$\Delta_{0,9spall}$	mid span displacement at 90% of P_{spall} in the post-peak response
Δ_w	evaporable water
ρ_l	density LWAC
ρ	oven-dry density of light weight aggregate concrete, $\rho = \rho_l - \Delta_w$
αd	depth of the compressive zone (depth of the neutral axis)
ε	strain
ε_c	concrete compressive strain
ε_{lcu}	ultimate compressive strain in LWAC
$\varepsilon_{lcu,c}$	ultimate compressive strain in confined LWAC
ε_s	strain in the tensile reinforcement
ε_t	transversal strain
σ_c	concrete compressive stress
σ_s	tensile stress in the tensile reinforcement
σ_2	transversal concrete compressive stress due to confinement
ν	poisson's ratio
κ	curvature at a particular section ($\kappa = 1/r = M/EI$)
Θ	angle of rotation

Definitions

CL	centre line
CMOD	crack mouth opening displacement
EI	bending stiffness
IT	inductive transducer (LVDT)
LVDT	linear variable differential transformer
LWAC	lightweight aggregate concrete
NA	neutral axis
NDC	normal density concrete
SG	strain gauge

1 Introduction

Lightweight aggregate concrete (LWAC) has been used as a construction material for many decades. The main objective for using LWAC is normally to reduce cost by reducing the dead load of structures. E.g. with low weight the dimensions of the foundations in buildings can be reduced in areas with low bearing capacities, the inertia actions are reduced in seismic regions and it enables easier handling and transportation of precast elements. Even with the major advantage of reduced weight and the high strength-to-weight ratio of the material compared to conventional concrete, the use of LWAC is still limited as a mainstream construction material in the building industry. However, for large and advanced structures like high rise buildings, bridges and offshore structures it has been applied with great success [1]. Other advantages of LWAC compared to normal weight concrete are the improved durability properties, fire resistance and the low thermal conductivity.

The major disadvantage of LWAC is the brittleness in compression at the material level compared to normal density concrete. Adequate strength, which easily can be fulfilled with lightweight concrete, is not the only required design criteria. In overload situations adequate ductility is essential to ensure safety. Ductility is defined as individual structural members or entire structures ability to sustain significant inelastic deformations after peak load without a significant loss in the capacity prior to failure. This is of great importance in redistribution of forces and a major consideration in design of structures in seismic areas. The limited post peak behaviour of LWAC can explain the limited use of the material for practical purposes. Requests for energy dissipation and/or a controlled behaviour after peak load can therefore exclude LWAC as the preferred material.

The main differences between the stress-strain diagrams of normal weight concrete and LWAC, characterized by a more linear ascending branch and a steeper descending branch, is rather well known, but the actual break-down of the sections involving splitting failure with loss of concrete cover is more uncertain.

It is well known that confinement increases the ductility of concrete in addition to enhancing the concrete strength. Active confinement from external stresses is more effective than passive confinement which is mobilised by opposing transverse deformation from the Poisson effect. In reinforced concrete the passive confinement from transverse reinforcement is the most common. Numerous researchers have investigated both experimental and theoretical, the effect of ordinary transverse steel reinforcement and the effect of adding fibres on the confinement in normal density concrete [2-6]. For lightweight aggregate concrete similar effects is reported [7-9]. The effect of confinement is also taken into account in design codes for concrete structures [10]. However, most studies on confinement focus on columns and cylinders subjected only to uniaxial loading [11-13]. Flexural behaviour of LWAC beams with focus on ductility has been reported, but only on under-reinforced beams [14-18].

This study focuses on ductility in compartment type of structures of reinforced lightweight concrete. Examples of economical feasible and where LWAC will be advantageous are floating offshore structures and temporary floating ground based structures, such as LNG-terminals. A major consideration in such structures is to avoid uncontrollable leakage of the compartments. Thus, they are post-tensioned to keep control of the cracking in service life. Preliminary studies of rectangular compartment structures subjected to horizontal excitation from earthquakes indicate that such stiff box structures have to resist the dynamic in-plane forces more or less elastically without significant energy dissipation in order to maintain the structural integrity and avoid uncontrollable leakage of the compartments. However, when the structure is subjected to vertical excitation, especially the continuous top slab carrying heavy equipment, the structure may be subjected to high g-forces with bending moment

reversals if the response is elastic. The maximum acceleration and dynamic forces may be significantly reduced provided that the structure has sufficient energy dissipation ability. The energy dissipation in flexure is mainly related to the yielding (and yielding reversal) of the reinforcement, but the stress-strain characteristics of the concrete in compression play an important part in limiting the amount of yielding possible before break-down of the plastic zones. Hence, the effect of confinement in the compression zone is of great importance.

The main objective in this study is to investigate the passive confinement effect of closed links and/or steel fibres on the ductility in LWAC structures. An experimental program was set up consisting of eight concrete beams, which were subjected to four-point bending. Four different configurations of the beams were investigated to study the response of only LWAC in the compression zone, steel fibre reinforcement, stirrups, and a combination of steel fibres and stirrups. The influence of the concrete compressive characteristics on the amount of reinforcement yielding is more pronounced in structures subjected to combined bending moment and axial force. Instead of introducing an axial force by post-tensioning the beams, they are heavily over-reinforced to focus on the compressive behaviour.

This experimental program is considered a first step on investigating the ductility of LWAC structures. Only static loading is considered, even if repeated loading is very important to assess structural integrity in seismic areas. Confinement and ductility of LWAC in general is well documented in the literature. However, information dealing with ductility of over-reinforced LWAC structures in bending or structures subjected to combined bending and membrane action is limited. The experimental work has been carried out as part of two Master theses at the Department of Structural Engineering at the Norwegian University of Science and Technology [19, 20].

2 Experimental program

2.1 Overview – beam design

The test program was designed to study the ductility enhancement in heavily over-reinforced lightweight aggregate concrete beams provided by steel fibres and steel confining transverse reinforcement. The main focus was on the ductility in the compression zone. Thus, the beams were heavily reinforced to ensure a bending failure in compression zone of the cross section before yielding of the tensile reinforcement.

The experimental program consisted of eight simply supported concrete beams, which were tested in flexure under a four-point loading system. Hence, the central part of the beam is in pure bending which is the main focus in this work. The free span between the supports was 3.6 m. The two concentrated loads were applied symmetrical with a distance of 0.8 m. Four different configurations of the LWAC beams were investigated to study the response. Two beams only with LWAC were considered beams for reference. Two beams each had steel fibres and stirrups respectively. The final two beams had a combination of closed links and steel fibres. The experimental setup is given in Figure 2.1 and an overview of the test program is given in Table 2.1.

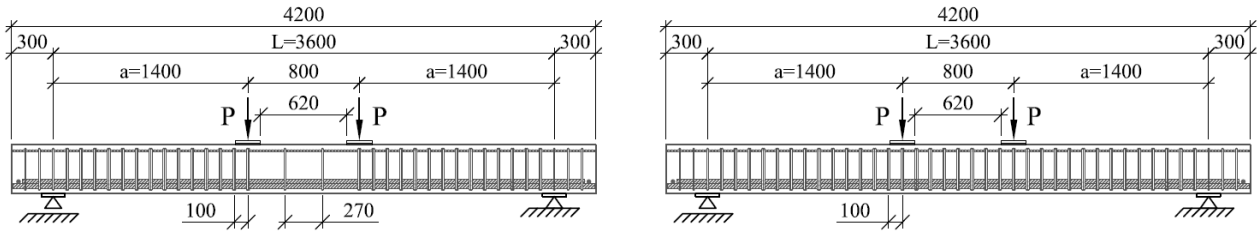

a) *Beam 1A/1B: Only LWAC*
Beam 2A/2B: Steel fibre

b) *Beam 3A/3B: Stirrups*
Beam 4A/4B: Steel fibre and stirrups

Figure 2.1*: Loading arrangement, confinement configurations and dimensions (in mm)*

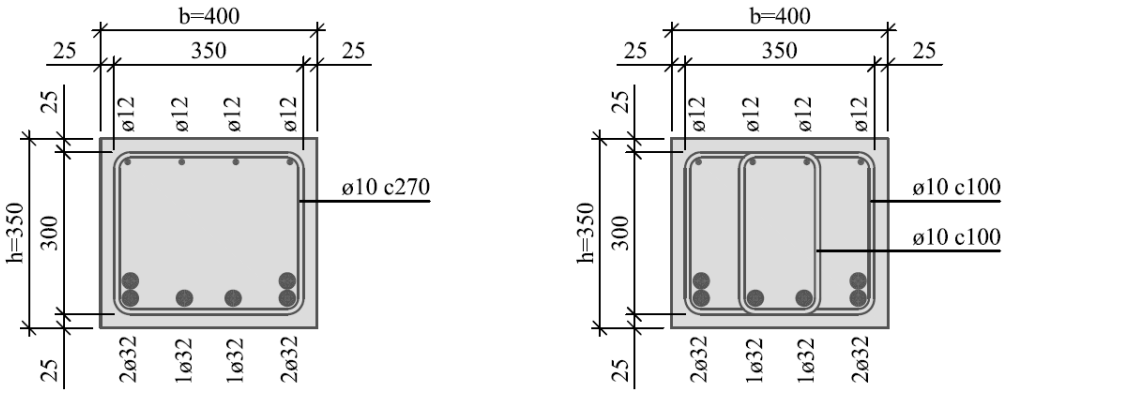

a) *Beam 1A/1B: LWAC only*
Beam 2A/2B: Steel fibre

b) *Beam 3A/3B: Stirrups*
Beam 4A/4B: Steel fibre and stirrups

Figure 2.2*: Reinforcement layout at mid span and dimensions (in mm)*

The cross sections in the beams were rectangular, 400 mm wide and 350 mm deep. The total length of the beams was 4.2 m and they were simply supported over a span of 3.6 m. The beams were designed to be over-reinforced, hence, the longitudinal tensile reinforcement should not yield at failure. To achieve this, six deformed bars with diameter 32 mm was required. They were arranged as 4 bars in a bottom layer and bundles of two bars at each side, as seen in Figure 2.2. In the compression zone 4 bars with diameter 12 mm was placed

in one layer. To ensure enough anchoring capacity a transverse horizontal bar with diameter 32 mm was welded on the bottom layer of the tensile reinforcement at the ends of the beams.

Transverse reinforcement consisted of 10 mm diameter deformed bars bent into closed stirrups. The concrete cover to the stirrups was 25mm. The aim of this work is to study the ductility in compression. Thus, in the shear spans between the load point and the support all beams were provided stirrups with spacing 100mm to ensure flexural failure. To avoid shear failure both an external and an internal stirrup was employed in each section, as seen in Figure 2.2 b). For beam type 3 and 4 intended for investigating the influence of stirrups on the ductility, the same combination of internal and external stirrup with spacing 100 mm were used in the flexural zone between the two concentrated loads. In beam type 1 and 2 only two outer stirrups were placed in the flexural zone to avoid buckling of longitudinal compression reinforcement and can be considered spreader bars. These two stirrups only have minor influence on the result, i.e. have no effective confinement effect due to a large centre distance of 270 mm, see Figure 2.1 a).

In production of the beams one batch of concrete was required per beam. The beams with only LWAC were casted using a “tobb”, while the beams with steel fibres used wheelbarrows to pour the concrete. In order to obtain sufficient distribution and increase the flow rate of the concrete, ladles were used to transport concrete along the beams. However, this influences the fibre distribution and orientation, especially in the top layer of the cross section. The concrete was compacted manually by sticks, with aluminium plates along the formwork, and by knocking the formwork with a rubber mallet. After casting the beams were stored in the formwork under polyethylene sheets to prevent moisture loss. One day later demoulding took place and the beams were again covered with wet burlap sacks and polyethylene sheets to prevent rapid moisture loss. Three days before testing the covers were removed to prepare the beams for testing.

***Table 2.1**: Testing program*

Configuration	Beam no.	Tensile reinforcement			Compression reinforcement			Testing age, t_0 (days)
		Bars	A_s (mm^2)	A_s/bd [1)]	Bars	A_s' (mm^2)	A_s'/bd [1)]	
Only LWAC	1A 1B	6ø32 —"—	4825 —"—	0,042 —"—	4ø12 —"—	452 —"—	0,004 —"—	28 29
Fibre	2A 2B	—"— —"—	—"— "—	—"— —"—	—"— —"—	—"— —"—	—"— —"—	29 30
Stirrups	3A 3B	—"— —"—	—"— —"—	—"— —"—	—"— —"—	—"— —"—	—"— —"—	29 29
Fibre + stirrups	4A 4B	—"— —"—	—"— —"—	—"— —"—	—"— —"—	—"— —"—	—"— —"—	30 30

[1)] Based on a fixed effective beam depth, d = 285 mm

***Figure 2.3**: Beam 1A casted and beam 1B prepared for casting*

2.2 Materials and mix proportions

The LWAC in the project were designed and prepared in-house. To produce the concrete, lightweight expanded clay aggregate, commercially known as LECA, was used to achieve the desired density of the LWAC. The project aimed for a mean compressive strength of ~ 35 MPa and a density of the LWAC of ~1800 kg/m^3.

The concrete mix is given in Table 2.2. The mix was the same for the A and B beams in each configuration, except for Beam 2 where a minor change in the mix was necessary due to a different supplier of the sand. The LECA 2-4 and 4-8mm have bulk densities of 380 kg/m^3 and 800 kg/m^3 respectively. To improve paste/cement and fibre/concrete bonds the mix contains silica fume of 9 % by weight of the cement. In addition limestone powder was added to avoid segregation. The sand had a high content of fines to increase the workability and to stabilise the concrete. For beams with steel fibres, Dramix 65/60 was used, which is a cold drawn wire fibre of bright steel with hooked ends and a length of 60 mm. The tensile strength of the fibres was 1000 MPa. The fibre content was 78 kg/m^3, which corresponds to an amount of fibres of 1 % by volume of concrete.

The moisture content and the absorbed water in the LECA were measured, and are necessary input when designing the concrete mix. After casting of beam type 1, there were some uncertainties on the moisture distribution in the LECA. The two fractions of LECA were then homogenised in a drum and sealed in plastic bags. Thus, the LECA in each concrete batch have almost the same moisture content.

***Table 2.2**: Concrete mix proportions for LWAC*

Constituent	Weight [kg/m^3]			
	Beam 1	Beam 2	Beam 3	Beam 4
Cement (CEM I)	430,0	428,1	428,5	428,8
Silica fume	38,7	38,5	38,6	38,6
Limestone powder	8,6	8,6	8,6	8,6
Water (free)	192,8	192,0	192,1	192,3
Absorbed water	36,9	2,3	6,5	2,3
LECA 2-4mm	148,9	179,4	173,5	176,3
LECA 4-8mm	198,6	239,2	236,9	235,1
Sand 0-8mm	708,8	774,9	767,8	781,8
Superplasticiser	7,7	4,7	6,2	4,7

The mixing was done using a 0.8 m^3 laboratory mixer. First cement, silica fume, LECA and sand were mixed for approximately 2 min. Water was added and the superplasticiser was continuously added and adjusted during mixing, until the desired workability of the concrete was achieved. Finally, steel fibres were carefully spread in the mixer to achieve a uniform distribution of the fibres in the concrete.

2.3 Mechanical properties

2.3.1 Properties in compression, LWAC

Mechanical properties were obtained for the LWAC for the different batches. For each beam six cylinders with diameter 100 mm and height 200 mm were casted to find the compressive strength and density of LWAC both after 28 days (water stored cylinders) and at the day of testing (cylinders stored together with the beams). The strength and the density were found according to the standards in [21] and [22] respectively. Table 2.3 presents the mean mechanical properties from tests at the same day as testing of the large beams.

***Table 2.3**: Mechanical properties for different mixes*

Beam no. and configuration	f_{lcm} (MPa)	E_{lcm} (MPa)	ε_{c0} (‰)	Density, ρ_l (kg/m^3)	Oven-dry density, ρ (kg/m^3)	f_{R3} (MPa)
1A: Only LWAC	36,9	-	2,32	1759	1560	
1B: Only LWAC	39,7	19,0	-	1812	1610	
2A: Steel fibre	34,9	-	2,30	1818	1620	
2B: Steel fibre	39,6	18,3	-	1881	1680	6,4
3A: Stirrups	34,5	-	2,04	1798	1600	
3B: Stirrups	33,5	20,0	-	1822	1620	
4A: Steel fibre + stirrups	27,7	-	2,00	1783	1580	
4B: Steel fibre + stirrups	40,4	18,0	-	1827	1630	7,0

The variation in compressive strengths within each beam configuration can partly be explained by differences in density. The beams with largest density also have the largest strength. However, for beam type 3 it is the opposite result, but here the differences in density and strength are smaller than for the other beam types.

From Table 2.3 it can be seen that the compressive strength varied relatively much considering the equal w/b-ratio of the mixtures. Especially for beam 4A and 4B the variation is large. One reason for the difference is the variation of degree of compacting, i.e. air content, due to the fibre content, expressed by the variation in the density of the hardened concrete. By assuming that every percentage of air content change gives a compressive strength reduction of 5 %, it can be demonstrated for beam 2A and 2B that some of the compressive strength differences are the results of different degree of compaction:
$39{,}6 \text{ MPa} \cdot 0{,}95^{[(1-1620/1680)\cdot 100]} = 33$ MPa, i.e. fairly equal to 34,9 MPa (Beam 2A).

The variation in mechanical properties between different batches was confirmed in testing of the beams, where beam 4A had the lowest capacity with regard to spalling. Also the obtained stress-strain relationship for the mixture from beam 4A confirms the low compressive strength, see Figure 2.4 d).

For half of the beams (beam 1B, 2B, 3B and 4B) Young's modulus of elasticity was found by following the procedure in [23] by employing three cylinders with height 200mm and diameter 100mm. Table 2.4 gives the mean mechanical properties obtained from the tests together with values in accordance with EC2. The tests were performed at the same day as testing of the beams. As seen the obtained E-modulus are in close agreement with EC2. The factor η_E, defined in EC2 as $(\rho/2200)^2$, is the ratio between Young's modulus of elasticity for lightweight and normal density concrete of the same concrete class.

***Table 2.4**: Tests Young's modulus of elasticity*

Beam no.:	**1B**	**2B**	**3B**	**4B**
f_{lcm} [MPa]	41,1	39,9	35,2	39,0
ρ [kg/m^3]	1610	1680	1620	1630
η_E	0,536	0,583	0,542	0,548
Eurocode 2:				
E_{lcm} [GPa]	18,0	19,5	17,4	18,1
LVDT:				
E_0 [GPa]	18,0	17,8	19,5	17,0
E_c [GPa]	19,0	18,3	20,0	18,0

From one batch for each of the beam types (beam 1A, 2A, 3A and 4A), the compressive stress-strain relationships were found based on three cylinders with height 280 mm and diameter 100 mm and following the testing procedure described in [24]. Figure 2.4 presents the obtained stress-strain relationship for the LWAC with 0% and 1% of steel fibre. The results are mean values for three cylinders both from strain gauges (SG) and LVDT (IT). The stress-strain relationship according to EC2 is based on the oven-dry density. Compared to the test curves from IT and SG, the EC2 curves are always between these curves. The fibres have a significant effect on the descending part of the relationship. This is in agreement with results reported in the literature [26-28]. However, the effect of fibres on the ductility in the cylinders is much less than the effect observed in the compressive zone of the full scale beams, see Chapter 3 and 4. Since the testing was performed on cylinders from different batches it is difficult to conclude on the effect of fibres on the compressive strength. In general fibres increase the compressive strength [9, 28, 29], but decreases in strength has also been reported [30]. The influence of fibres strongly depends on the amount, dispersion and type of fibre, aggregate type and size, workability of the concrete and degree of compacting achieved. However, in this work ductility is the main focus and the compressive strength of minor interest.

Table 2.5 gives the details from the obtained stress-stress relationships and values defined in EC2. The ultimate strains, ε_{lc1}, in EC2 when applying the stress-strain relationship for non-linear analysis, are in satisfactory agreement with the measured ultimate strains, ε_{c0}, especially from the LVDT. The parameter *m* is the relationship between the secant modulus at 60% of the failure load, E_{cn60}, and the secant modulus at failure. It is a measurement on the ductility and degree of non-linearity of the stress-strain relationship. As expected for LWAC the parameter is quite small. Poisson's ratio at 40% of the ultimate capacity, ν_{40}, varies between 0,21 and 0,23. There is no observed effect of fibres on the ratio. This can partly be explained by the low load level and the long fibres which are of the same magnitude as the diameter of the cylinder.

***Table 2.5**: Test results from stress-strain relationship*

Beam no.:	**1A**	**2A**	**3A**	**4A**
f_{lcm} [MPa]	34,3	35,1	30,3	26,6
ρ [kg/m^3]	1560	1620	1600	1580
η_E	0,503	0,542	0,529	0,516
Eurocode 2:				
E_{lcm} [GPa]	16,0	17,4	16,2	15,2
k	1,10	1,10	1,10	1,10
ε_{lc1} [‰]	2,36	-2,22	-2,06	-1,92
ε_{lcu3} [‰]	2,89	2,95	2,93	2,91
LVDT:				
E_{cn40} [GPa]	16,5	17,1	16,7	14,8
E_{cn60} [GPa]	16,1	16,7	16,3	14,5
m	1,09	1,10	1,10	1,09
ε_{c0} [‰]	2,32	2,30	2,04	2,00
Strain gauges:				
E_{cn40} [GPa]	18,9	19,1	19,2	16,5
E_{cn60} [GPa]	18,5	18,7	18,8	16,1
m	1,11	1,11	1,10	1,10
ε_{c0} [‰]	2,08	2,08	1,77	1,83
ν_{40}	0,23	0,23	0,22	0,21

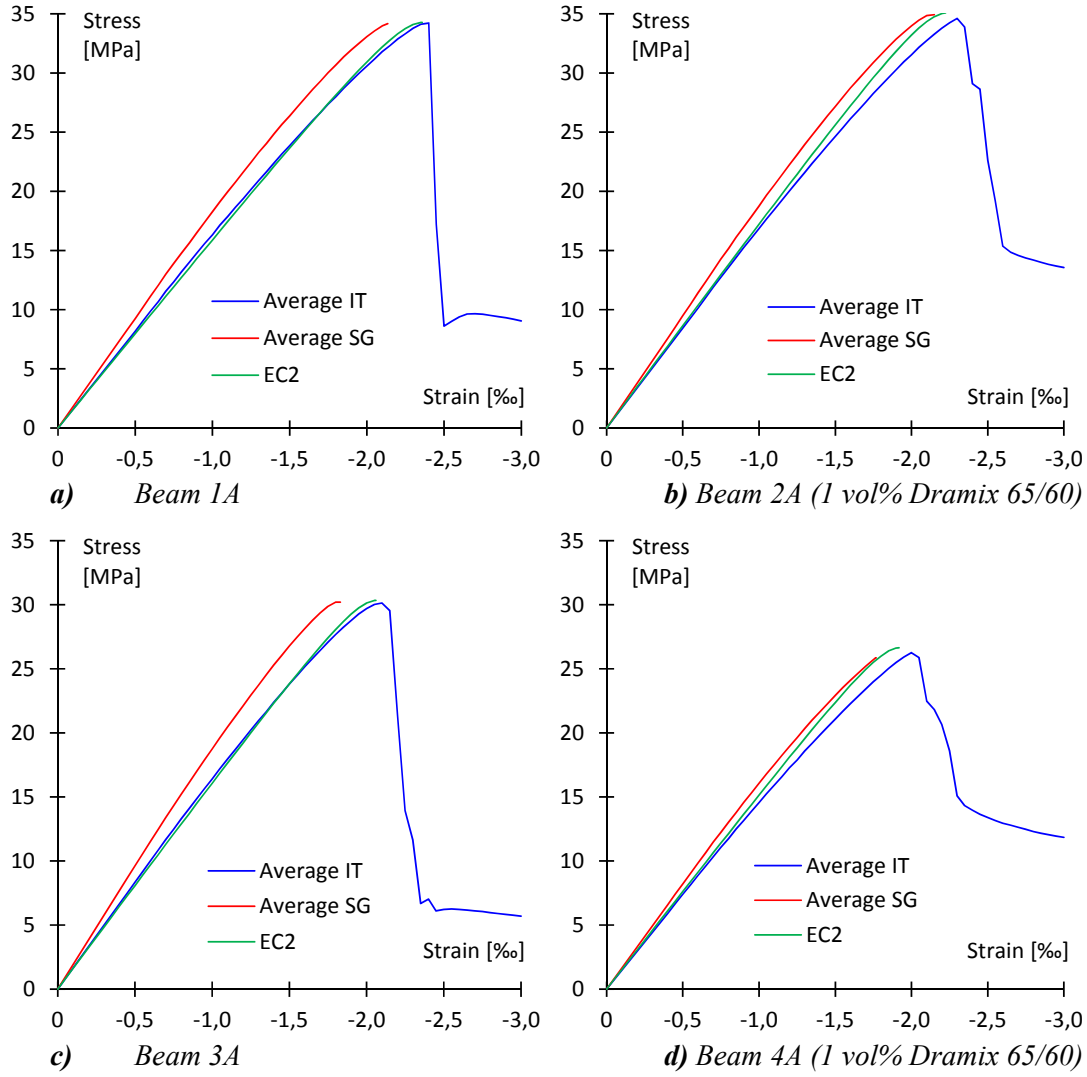

a) *Beam 1A* ***b)*** *Beam 2A (1 vol% Dramix 65/60)*

c) *Beam 3A* ***d)*** *Beam 4A (1 vol% Dramix 65/60)*

Figure 2.4*: Stress-strain relationships for lightweight aggregate concrete*

2.3.2 Residual flexural tensile strength, FRLWAC

For the two configurations of beams with steel fibre, beam 2B and 4B, six small scale beams were casted from the same concrete batch as the large beams, to investigate the residual flexural tensile strength in accordance with [31]. The tests are based on simply supported beams with a free span of 0.5 m and a square cross section of 0.15 m, subjected to three point bending. The beams have a 25 mm deep notch at the middle point to initiate cracking. The results are presented in Figure 2.5 by using the crack mouth opening displacement (CMOD). In bending design of steel fibre reinforced concrete structures the residual flexural strength at a $CMOD_1$ of 2.5 mm, f_{R3}, is often used [32, 33]. The mean values of f_{R3} were 6.4 MPa and 7.0 MPa, with a relative standard deviation of 25% and 15 % for the two series respectively, see Table 2.6.

***Table 2.6**: Flexural strength and residual flexural strength at testing (MPa)*

	Small scale beam no.	X1	X2	X3	X4	X5	X6	Mean value	Std. (%)
Beam 2B	Max flex. str. $f_{R,max}$	4,2	7,8	9,0	6,7	9,1	6,6	7,2	25,7
	$CMOD_1$: Res. flex. str. f_{R1}	4,0	6,2	8,8	6,4	9,0	5,9	6,7	28,3
	$CMOD_2$: Res. flex. str. f_{R2}	4,1	6,3	8,8	6,5	8,1	6,5	6,7	24,6
	$CMOD_3$: Res. flex. str. f_{R3}	3,9	5,8	8,8	6,3	7,2	6,2	6,4	25,1
	$CMOD_4$: Res. flex. str. f_{R4}	3,8	5,5	8,4	6,0	6,9	5,7	6,0	25,7
Beam 4B	Max flex. str. $f_{R,max}$	7,5	7,4	9,6	8,1	7,5	8,4	8,1	10,4
	$CMOD_1$: Res. flex. str. f_{R1}	7,4	7,3	8,5	4,2	7,3	8,3	7,2	21,4
	$CMOD_2$: Res. flex. str. f_{R2}	7,1	6,5	9,6	8,1	7,4	7,7	7,7	13,7
	$CMOD_3$: Res. flex. str. f_{R3}	6,5	5,9	9,0	7,1	6,6	6,8	7,0	15,2
	$CMOD_4$: Res. flex. str. f_{R4}	6,0	5,4	8,3	6,3	6,3	6,5	6,5	14,7

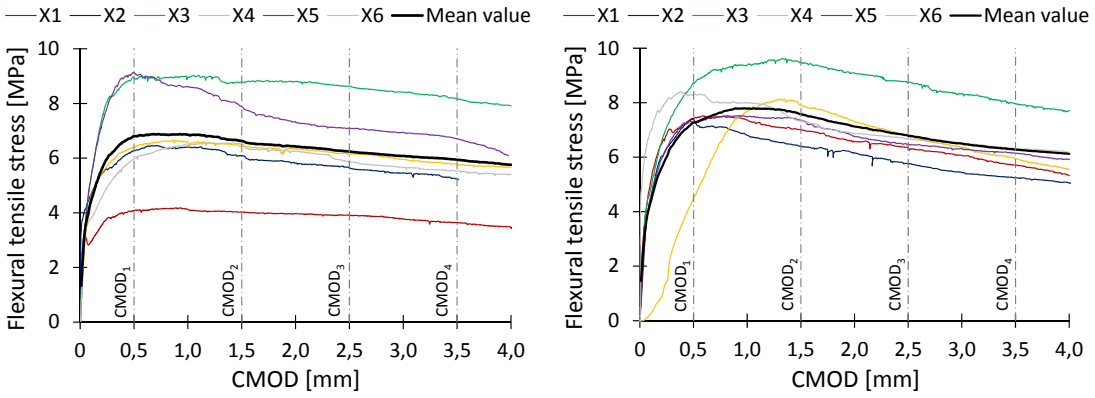

***a)** From beam 2B (1 vol% fibre)* ***b)** From beam 4B (1 vol% fibre)*

***Figure 2.5**: Flexural tensile strength - CMOD diagrams*

The large scatter of results in Figure 2.5 is an indication on poor dispersion of the fibres in the beams. The fibre distribution in the cross-section was found by counting the number of fibres in a 25 mm top layer, a 100 mm middle layer and a 25 mm bottom layer of the cross-section, see Appendix A7. The mean values for the number of fibres varied between 0.61 pr cm^2 for the top layer to 1.22 pr cm^2 for the middle layer. However, only the numbers of fibres were registered. No attempt was made to find a fibre orientation factor.

2.3.3 Reinforcement

The beams in this project are over-reinforced. Hence, the yield strain and Young's modulus of elasticity of the longitudinal reinforcement are important parameters. To be able to evaluate the results and to compare the strains from the experiments with calculations, deformed bar with diameters 10 and 32 mm were tested according to [34] to characterize the properties. Figure 2.6 shows the stress-strain relationships from the tests as mean values for three tests. The bar with diameter 10mm has an almost perfect linear-ideal plastic behaviour. As expected the bars with diameter 32mm shows a more non-linear behaviour before reaching the yield stress at a strain of 3.75‰. Table 2.7 summaries the results from the testing. Young's modulus of elasticity is calculated from the linear part of the stress-strain diagram.

***Table 2.7**: Mechanical characteristics of reinforcement steel*

Bar diameter (mm)	Yield stress (MPa)	Yield strain (mm/m)	Young's modulus (GPa)
10	549	2,76	199
32	565	3,75	188

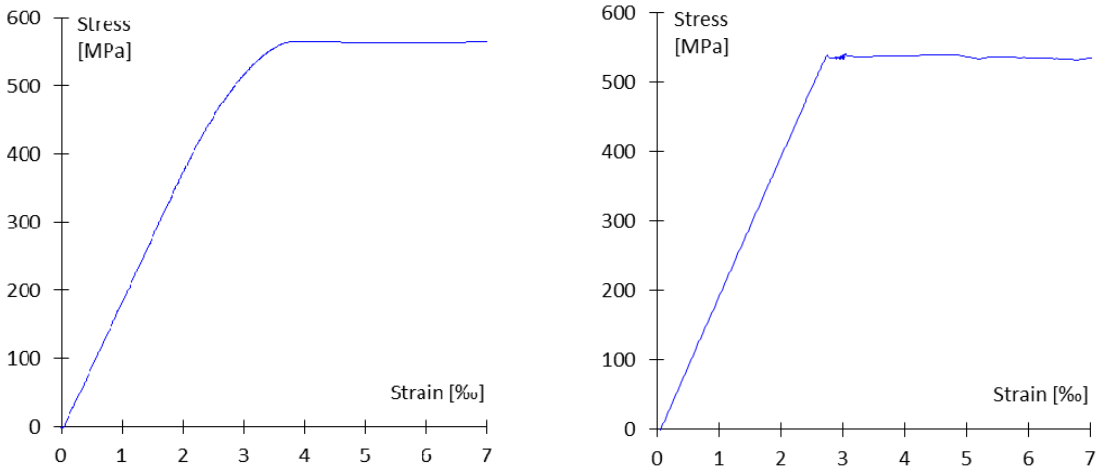

***a)** Reinforcement, ø32* ***b)** Reinforcement, ø10*

***Figure 2.6**: Stress-strain relationships for reinforcement*

2.4 Instrumentation and test procedure

The beams were suitable instrumented to measure displacements and strains, see Figure 2.7 – 2.9. Deflections of the beams were measured at mid span and at the load transfer points by three vertical linear variable differential transformers (LVDT), IT5-IT7. To capture the concrete strains four LVDTs were placed horizontally at the top and bottom level at both sides of the cross-section, IT1-IT4. They measured the longitudinal displacements over a distance of 0.5 m. Six strain gauges were used to measure the steel strains. In longitudinal direction two gauges were mounted at the two central reinforcement bars both in the top and at the bottom, SG1-SG4. Since validation of the confinement effect is one of the main objectives in this study, two strain gauges were used in the horizontal direction of the shear links at the top, SG5-SG6.

The load was applied by a 1000kN servo controlled hydraulic actuator, and distributed to the LWAC beam by a steel beam (equalizer beam) with two rolled supports, see Figure 2.7. As an initial stage the beams were preloaded with a very small load to remove any slack in the system. The load was then released and all instruments were zeroed. The beams were loaded at a rate of 1.0 mm/min. Up to load level 66,7 kN the loading was applied in intervals of 16,7 kN. Above 66,7 kN the intervals was doubled to 33,3 kN. At each load level there was a 5 min break to study the formation of cracks. After reaching load at spalling, the beams were continuously loaded. All displacement, strain and load readings were automatically logged with a rate of 0.5 Hz.

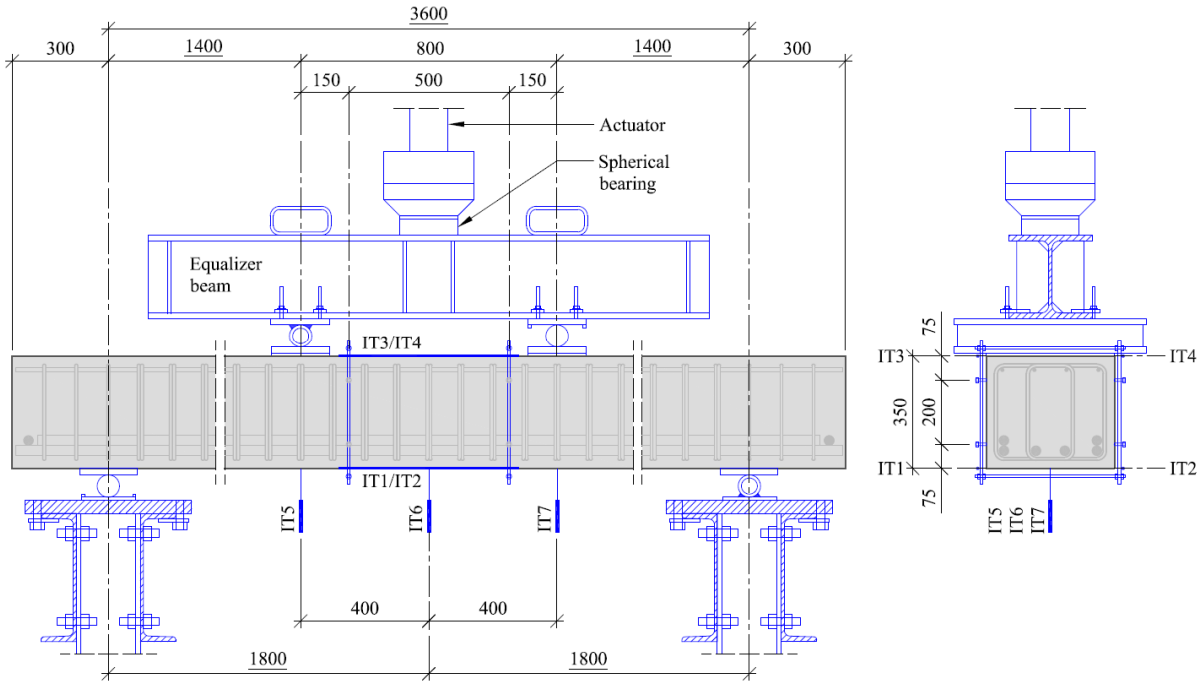

***Figure 2.7**: Loading arrangement and instrumentation*

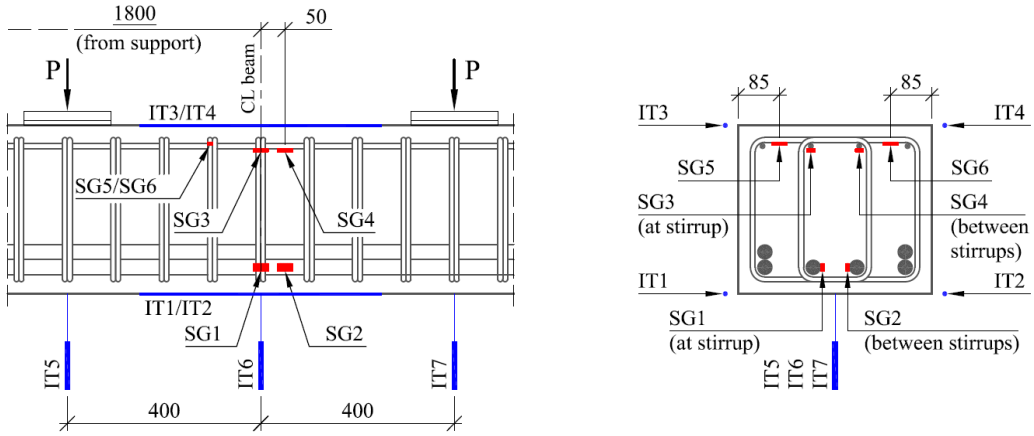

***Figure 2.8**: Instrumentation beam 1A/1B and 2A/2B. Strain gauges (SG1 to SG6) and linear variable differential transformers, LVDT (IT1 to IT7)*

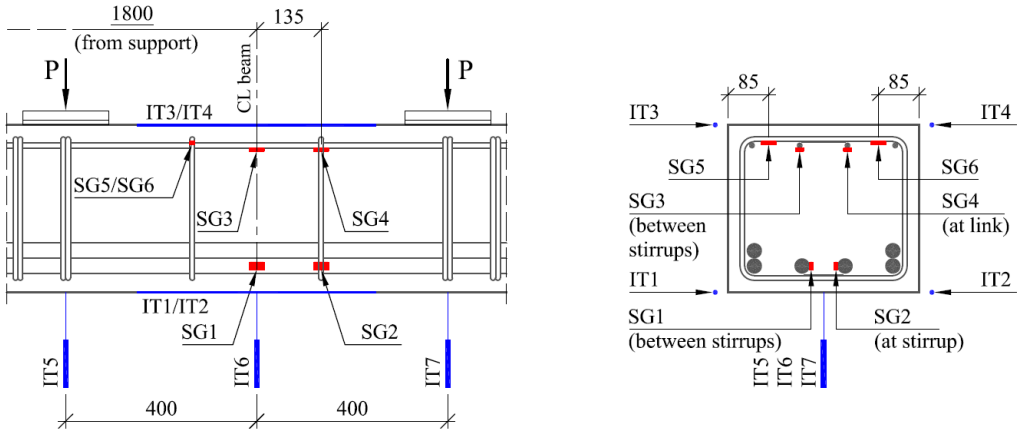

***Figure 2.9**: Instrumentation beam 3A/3B and 4A/4B. Strain gauges (SG1 to SG6) and linear variable differential transformers, LVDT (IT1 to IT7)*

3 Test results and discussion

3.1 Main results

Table 3.1 summaries the main experimental results and calculations of the full scale tests regarding load capacity and displacement at mid span.

***Table 3.1**: Main experimental results and calculations – Full scale experiments*

Configuration and beam no:		Material LWAC [1]		Experimental results, loads [2]					Experimental results, displacements at mid span [2]					Calculations, load capacity [3]				
		ρ [kg/m^3]	f_{lcm} [MPa]	P_{spall} [kN]	M_{spall} [kNm]	P_{peak} [kN]	M_{peak} [kNm]	P_{peak}/ P_{spall}	Δ_{spall} [mm]	Δ_{peak} [mm]	$\Delta_{0.9spall}$ [mm]	Δ_{peak}/ Δ_{spall}	$\Delta_{0.9spall}$/ Δ_{spall}	$P_{spall,calc}$ [kN]	P_{spall}/ $P_{spall,calc}$	$P_{peak,calc}$ [kN]	P_{peak}/ $P_{peak,calc}$
Only LWAC	Beam 1A	1560	36,9	280,9	399,9	154 [4]	221 [4]	0,549 [4]	24,8	[4]	[4]	[4]	[4]	288	0,98	182	0,85
	Beam 1B	1610	39,7	291,2	414,4	150 [4]	215 [4]	0,515 [4]	25,9	[4]	[4]	[4]	[4]	305	0,96	194	0,77
Steel fibre	Beam 2A	1620	34,9	281,1	400,2	282,9	402,7	1,006	23,9	26,0	37,2	1,09	1,56	278	1,01	174	1,63
	Beam 2B	1680	39,6	279,0	397,3	284,9	405,5	1,021	23,1	28,8	52,1	1,25	2,26	306	0,91	194	1,47
Stirrups	Beam 3A	1600	34,5	289,2	411,6	293,5	417,6	1,015	24,5	30,5	36,3 [5]	1,25	1,48 [5]	275	1,05	268	1,10
	Beam 3B	1620	33,5	279,0	397,3	278,4	396,4	0,998	23,9	29,5	39,5	1,23	1,65	270	1,03	261	1,07
Steel fibre + stirrups	Beam 4A	1580	27,7	253,1	361,0	280,5	399,4	1,108	22,0	34,2	100,7	1,56	4,58	235	1,08	217	1,29
	Beam 4B	1630	40,4	271,5	386,8	298,3	424,3	1,099	22,6	31,3	79,9	1,39	3,54	309	0,88	313	0,95

1) Mean values from Chapter 2.3.1 (used in calculations)
2) Load-displacement relationship, see figures in Chapter 3.2 and Appendix A1
3) Calculation according to Eurocode 2 [10], see Chapter 3.4. The fibre contribution to the ultimate compressive strain is not taken into account when calculating for P_{peak}
4) Not relevant due to brittle behaviour at spalling and drop in load capacity (no real peak load achieved)
5) Test terminated at $P \approx 0{,}94\ P_{spall}$

3.2 Load-displacement relationships

To investigate and describe the response of the tested beams, references will be made to the principal bending response of the over-reinforced concrete beams which is illustrated in Figure 3.1. The response can be characterized by five stages:

1. Before concrete cracks, 0-A
2. Linear response for a cracked cross-section, A-B
3. Non-linear response, B-C, before reaching the compressive capacity (strain limit) of the beam which initiate the spalling in the compressive zone, P_{spall}
4. A very brittle behaviour for beams with only LWAC, C-F, for beams with confinement in the compressive zone a redistribution of stresses which involve spalling of the concrete cover and reaching a second peak load P_{peak}, C-D
5. With confinement a ductile post–peak behaviour, D-E

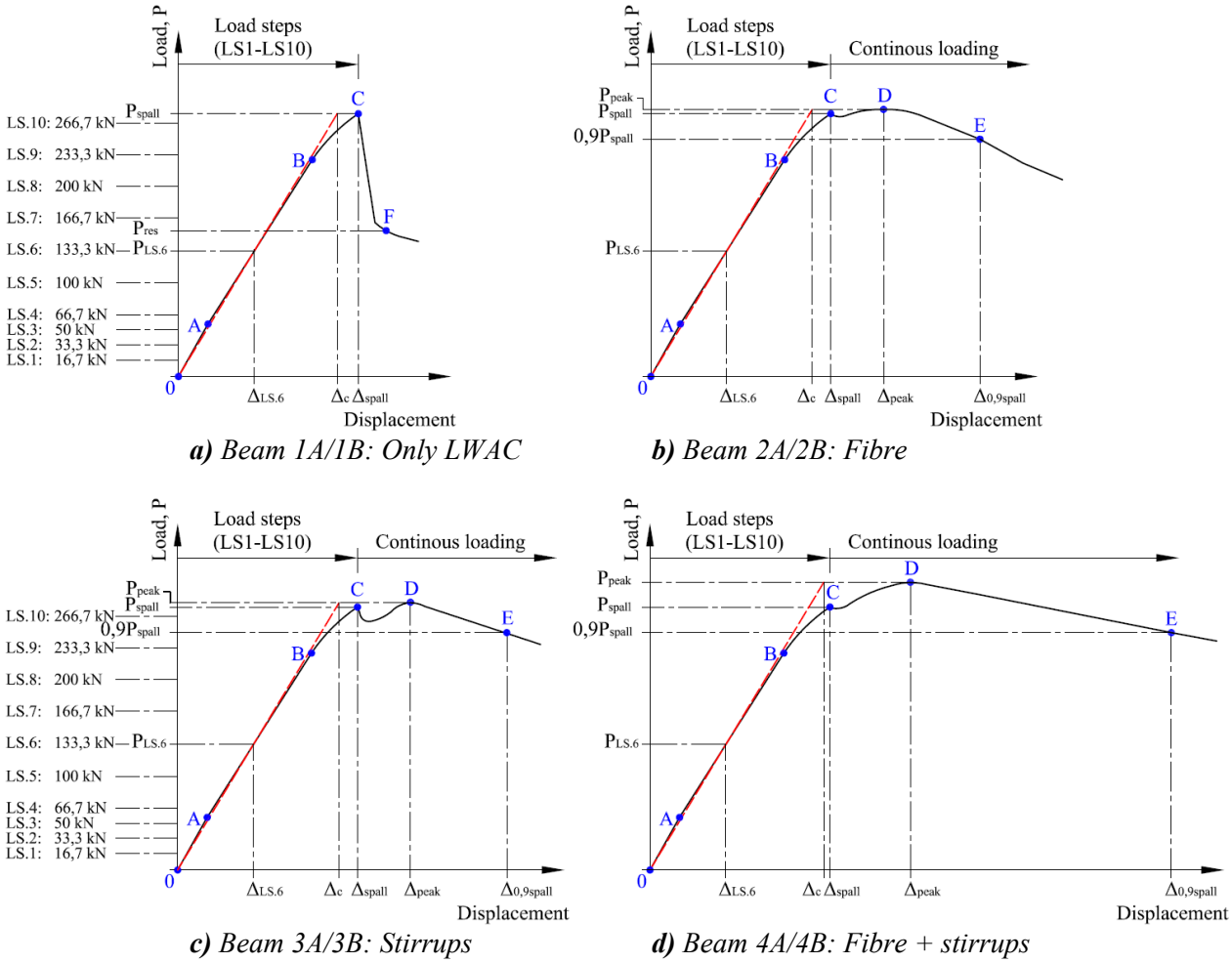

a) *Beam 1A/1B: Only LWAC*

b) *Beam 2A/2B: Fibre*

c) *Beam 3A/3B: Stirrups*

d) *Beam 4A/4B: Fibre + stirrups*

Figure 3.1*: Schematic load-displacement behaviour of the over-reinforced LWAC beams with different configurations in the compressive gradient zone.*

The load-displacement curves for the centre point are given in Figure 3.2 for all eight beams. As expected beams with only LWAC, beam 1A and 1B, have a very brittle response after reaching maximum capacity (load at spalling). The responses for the beams demonstrate the strong influence of the different confinement configurations on the behaviour at and after spalling. In the range 0 - C in Figure 3.1 there are no significant influence of the different

configurations, however some increased elastic bending stiffness can be identified by introducing confinement in the compression gradient zone, see Figure 3.2 a).

Beams with fibre, beam 2A and 2B, show a ductile response. After initiation of spalling the load capacity is levelled out with no increase in the capacity. In the post-peak behaviour, which includes a descending branch in the load-displacement response, the two beams show different response. In casting of the beams there were differences in workability of the concrete which influence fibre distribution and orientation However, even if registration of distribution and fibres were not performed this is an indication of the importance of fibre content on the compressive ductility.

Beams with shear reinforcement but no fibres, beam 3A and 3B, show a very clear unloading after the first peak load, associated with spalling of the concrete cover in the compression zone. However, the shear links are able to maintain a cross-section and after some redistribution of stresses a second peak point can be identified. After peak point the beams show ductile response analogous the beams with fibre.

Beams with fibre and stirrups, beam 4A and 4B, have a very ductile behaviour. They also experience a significant increase in capacity from load at spalling to peak load (about 10 %). Thus, the confinement effect from fibres and stirrups increase the compressive strength in addition to increased ductility. After peak load the beams are able to maintain a high load level with only a slight descending gradient.

Load-displacement curves and load-time curves, as illustrated in Figure 3.2 and 3.3 respectively, are shown separate for each beam in Appendix A1, where also the load and displacement at spalling and peak load are given.

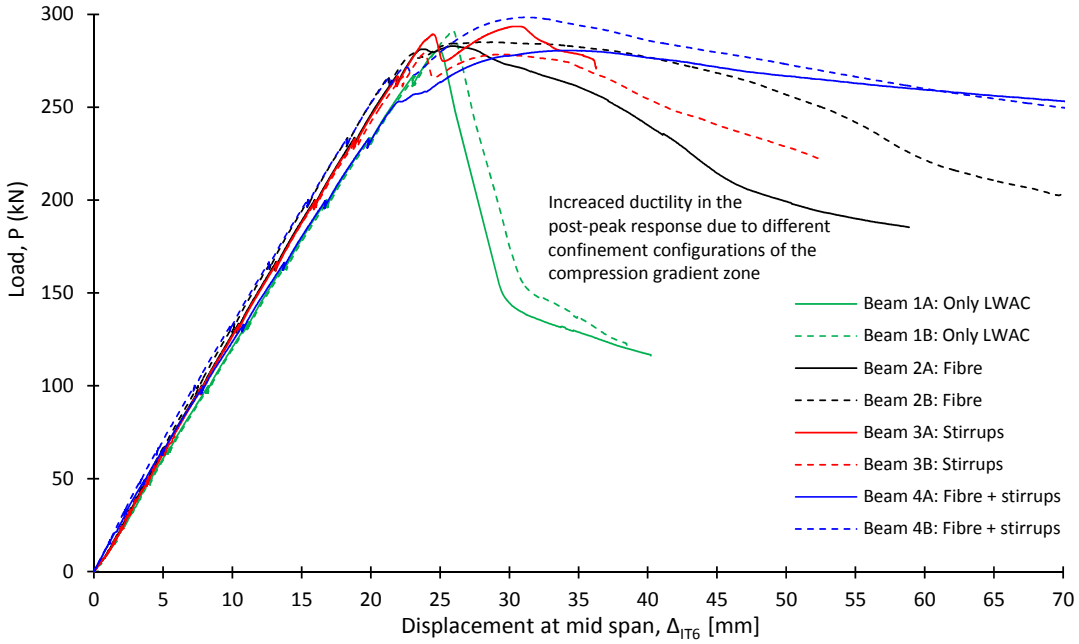

a) *Load-displacement curves*

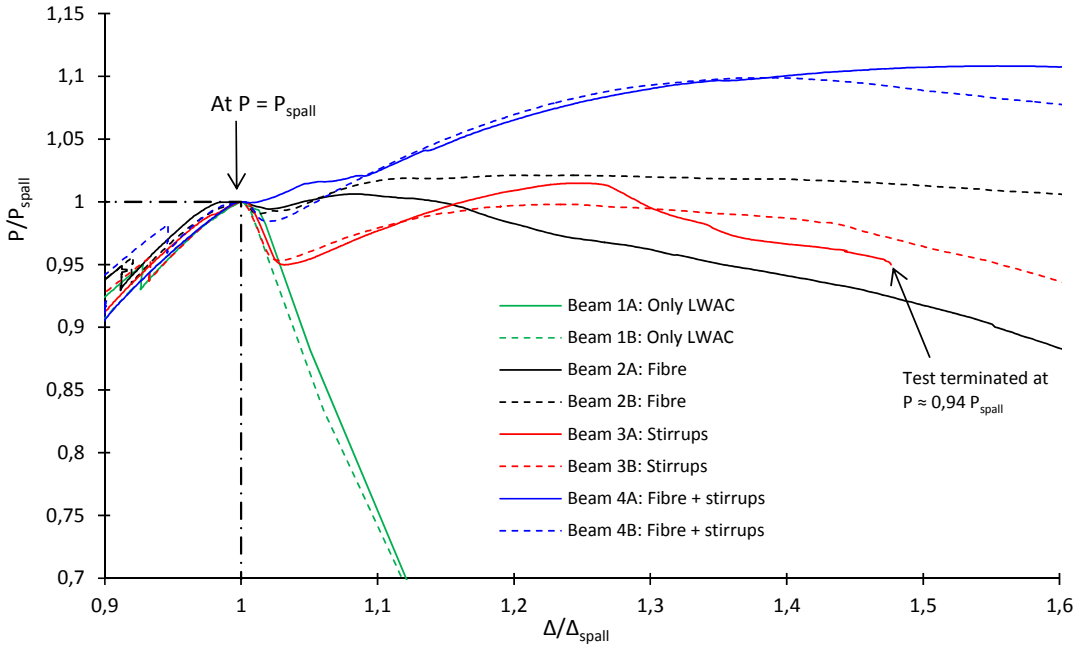

b) *Section of the normalized load-displacement curves around P_{spall}*

Figure 3.2*: Load-displacement curves for all beams at mid span*

As previously described the tests are performed with deformation controlled loading in load steps up towards spalling, and with continuous loading at- and after spalling. This loading procedure can clearly be seen in the load-time curves in Figure 3.3. The difference in load response between the beams at and after spalling, P_{spall}, are even clearer in the load-time curves than in the load-displacement curves. The load-time curve for beam 3A deviates from other beams due to load steps of 8,3 kN instead of 16,7 kN for the first two load steps. Hence, the load-time curve for beam 3A is delayed approximately 10 minutes compared to the other beams.

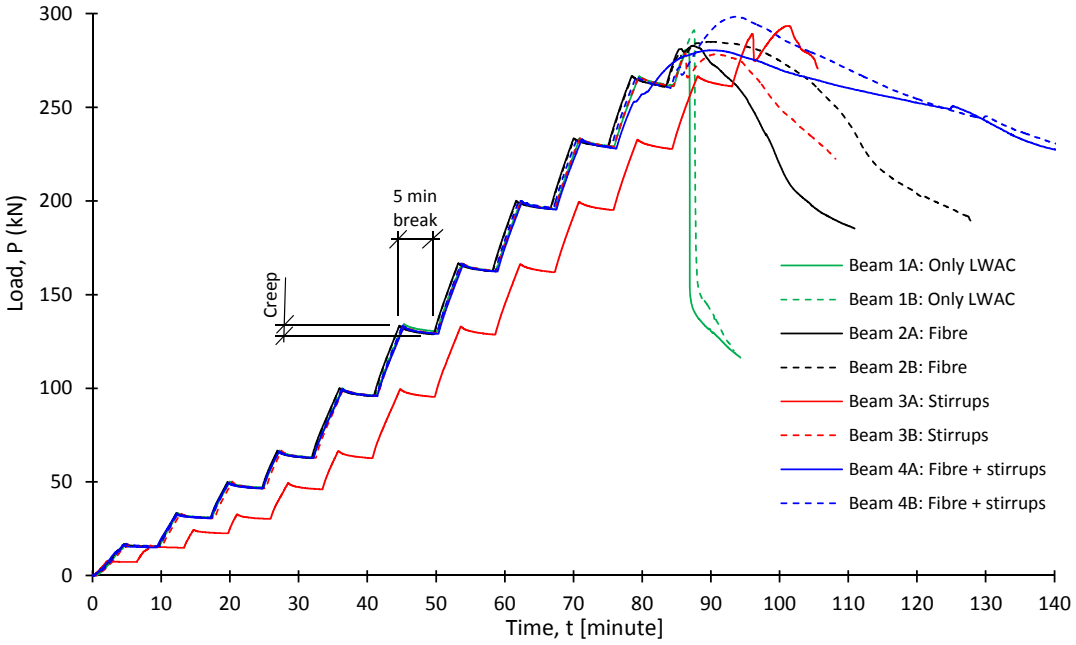

a) *Load-time curves*

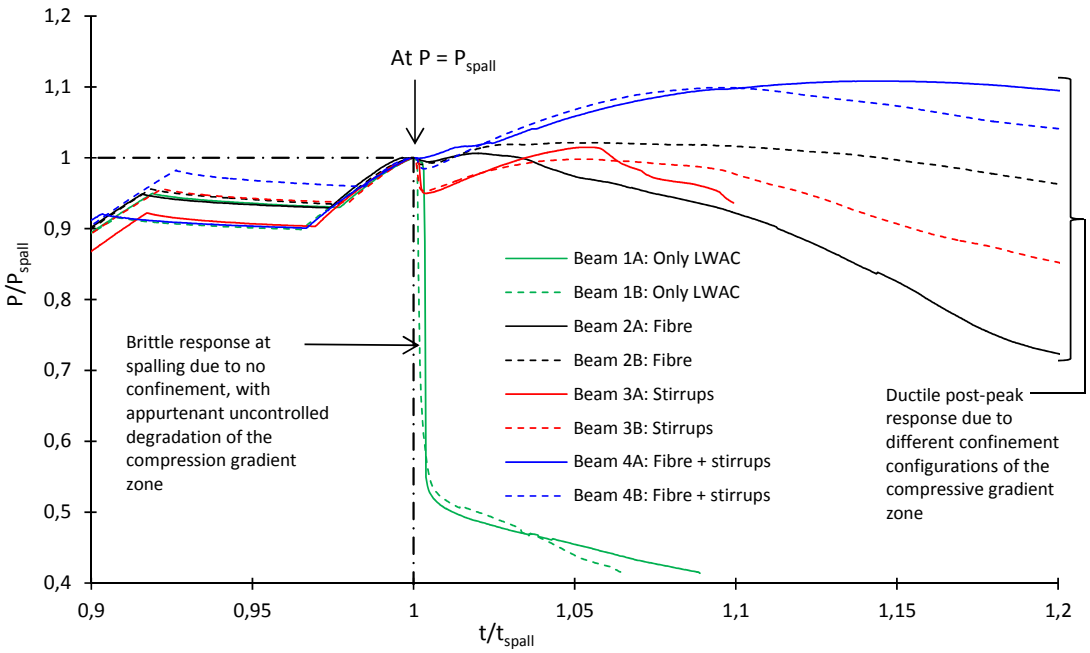

b) *Section of the normalized load-time curves around* P_{spall}

Figure 3.3*: Load-time curves for all beams*

3.3 Concrete and steel strains

3.3.1 Strain curves

Experimental moment-strain and time-strain relation for one reference beam with only LWAC, beam 1A, and for one beam with fibre and stirrups, beam 4A, are shown in Figure 3.4 and 3.5 respectively. Analogous to the load-displacement relationships shown in Chapter 3.2, Figure 3.4 and 3.5 show the significant improvement of the flexural response at spalling of the compression zone by introducing a combination of confinement from fibre and stirrups.

Figure 3.5 shows how fibre and stirrups, i.e. cross-section with confined fibre reinforced LWAC in the compression gradient zone, result in a very ductile behaviour at and after spalling. After reaching the spalling moment, M_{spall}, beam 4A is able to maintain and increase the bending capacity with corresponding large strains in the compressive zone. However, the moment-strain relations up to M_{spall} are not significantly influenced of the introduction of steel fibre and stirrups. The positive values show the compressive strains in the LWAC (IT3-IT4) and in the compression reinforcement (SG3-SG4), while the tensile strains in the reinforcement (SG1-SG2 and SG5-SG6) and at the bottom of the beams (IT1-IT2) are shown in negative values.

Strain curves for all beams are given in Appendix A2.

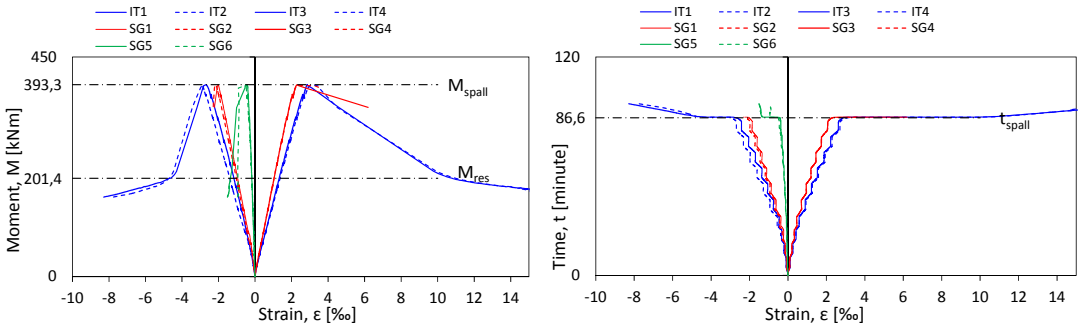

a) *Moment-strain curves* ***b)*** *Time-strain curves*

Figure 3.4*: Strain curves for Beam 1A, only LWAC.*

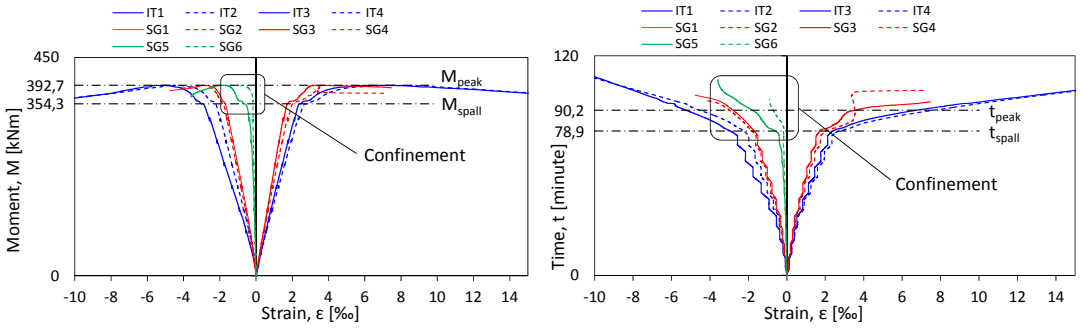

a) *Moment-strain curves* ***b)*** *Time-strain curves*

Figure 3.5*: Strain curves for Beam 4A, fibre + stirrups.*

3.3.2 Strain distribution in cross-section at peak-loads

The strain distributions in cross-section at spalling (P_{spall}) and at peak load (P_{peak}) are illustrated in front elevation for each beam in Figure 3.6 – 3.9. The corresponding lateral strains are shown in Appendix A3. The relation between transversal strains and longitudinal strains are typical in the range 0,2 – 0,3, i.e. a Poisson's ratio, *v*, around 0,2 at loads below spalling, and around 0,3 at spalling. A Poisson's ratio around 0,2 in the linear elastic stress-strain range in the compression zone of the beams is in agreement with values obtained on cylinders, see Chapter 2.3.1.

The calculated strain distribution at spalling, $P_{spall,calc}$, are also shown in Figure 3.6 – 3.9, and correspond quite well with the experiments, in the same way as the calculated capacity itself, i.e. the concrete compressive strain at spalling (from IT1 – IT4) correspond with the ultimate compressive strain, ε_{lcu3} (EC2), used in calculations.

For beam 1A and 1B in Figure 3.6 the strain distribution after spalling refers to the rest-capacity since no peak load was achieved. The brittle collapse of the compression gradient zone of these reference beams at spalling are evident with a rotation centre localized close to the centre of the longitudinal tensile reinforcement.

Strains in the reinforcement (SG1 – SG4) are local, while strains at the top and bottom surfaces of the beams (IT1 – IT4) represents average strains over a length of 500 mm, see Figure 2.7 – 2.9. Loading above P_{spall} introduces concentration of strains towards the middle of the span of the beam due to formation of a plastic hinge region. This can be observed from beams 2A/2B and 3A/3B since the strains in the compressive reinforcement increase more than the average strain at the top surface from P_{spall} to P_{peak}. Propagation of the plastic failure zone is closer investigated in Chapter 4.4.

Due to spalling, the strain gauges (SG3 and SG4) on the compressive reinforcement failed when approaching P_{peak} for Beam 1 and Beam 4, and no measurements are available. Strain measurements up to P_{spall} show a reasonable resemblance between strain gauges and LVDT's, i.e. the strain distribution is linear over the cross-section and evenly distributed across the middle 500 mm of the beams.

From Figure 3.6 – 3.9 it appears that the response from the tensile reinforcement is elastic all the way up to P_{peak} for all beams, i.e. the beams can be characterized as over-reinforced, also in the response from spalling to peak load. However, the compression reinforcement is yielding at P_{peak}, but not considered effective due to initiated buckling.

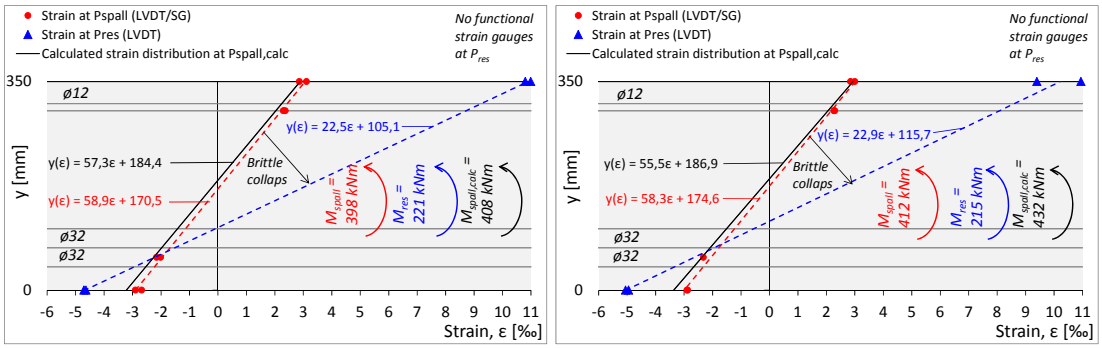

a) *Beam 1A* ***b)*** *Beam 1B*

Figure 3.6*: Beam 1A/1B – Only LWAC. Longitudinal strain distribution. Brittle collapse of the compression gradient zone from M_{spall} to M_{res}*

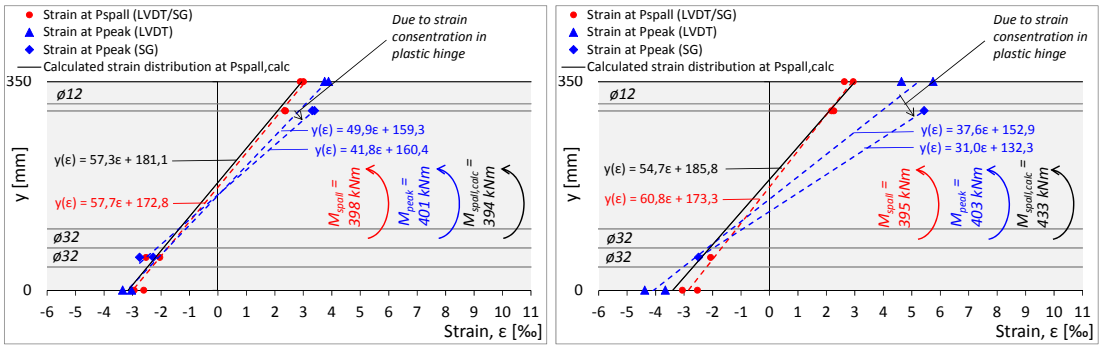

a) *Beam 2A* ***b)*** *Beam 2B*

Figure 3.7*: Beam 2A/2B – Fibre. Longitudinal strain distribution*

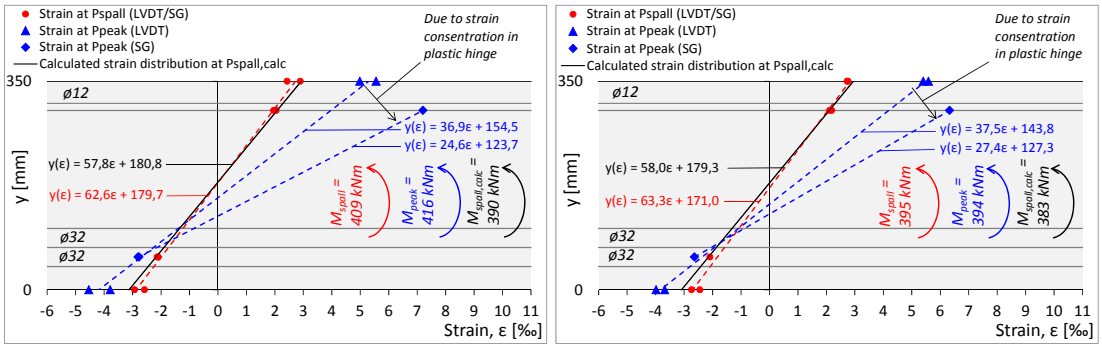

a) *Beam 3A* ***b)*** *Beam 3B*

Figure 3.8*: Beam 3A/3B – Stirrups. Longitudinal strain distribution*

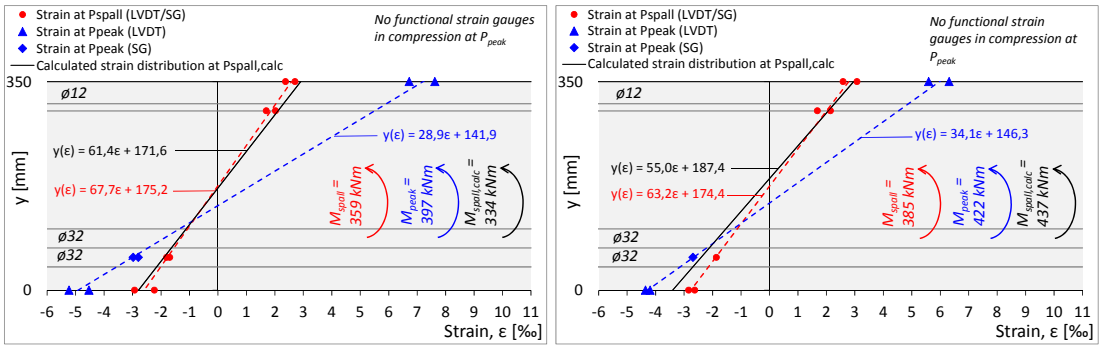

a) *Beam 4A* ***b)*** *Beam 4B*

Figure 3.9*: Beam 4A/4B – Fibre + stirrups. Longitudinal strain distribution*

3.4 Failure mode and ultimate strength

The governing failure mode for all beams was typical bending failures for over-reinforced beams. The failure and spalling of the concrete cover are initiated and identified when horizontal cracks occurs in the compression zone. Depending on the degree of confinement, pictures in Figure 3.10 – 3.12 shows the typical differense in the the failure zone between the reference beam with only LWAC (beam 1A) and beam with fibre and stirrups (beam 4A). The pictures are taken at the end of testing, i.e. after a steep descending branch at a displacement $\Delta = 40$ mm and load $P = 116$ kN for beam 1A, and after a gradual descending branch at a displacement $\Delta = 100$ mm and load $P = 228$ kN for beam 4A. For beams without steel fibres the spalling is much more severe than beams with fibres, where the cross-section remains much more intact. The failure zone without fibres is much more local and concentrated than with fibres where the zone is wider.

Figure 3.13 – 3.16 show pictures at $P = P_{peak}$ and at $P = 0{,}9 \cdot P_{spall}$ for one of each beam type 1-4, with an exeption for beam type 1 where the pictures are taken at $P = P_{res}$ and at the end of testing since no peak load was achieved. From the figures it is clear that the size of the spalling zone in the longitudinal direction is typically limited by the distance of 620 mm between the fibreboards in the pure bending zone. Thus, these plates work as external confinement with respect to spalling. From the pictures it can be seen that in beams without fibres, the concrete cover above the compressive reinforcement is almost separated from the beams at peak loads. For beams with fibres there are only minor horizontal cracking in the compressive zone at peak load.

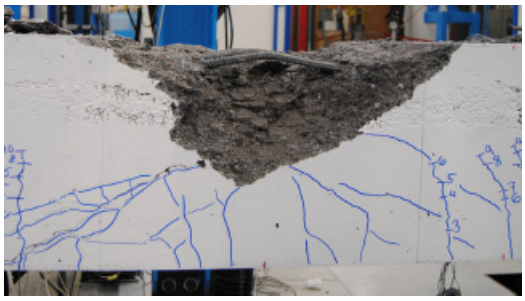

a) Beam 1A: Only LWAC

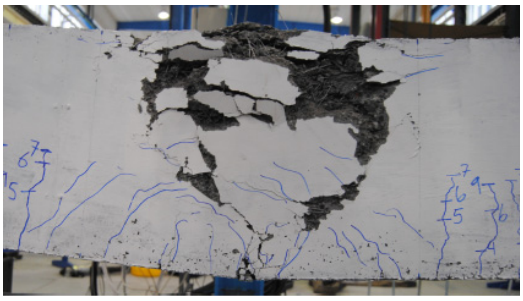

b) Beam 4A: Fibre + stirrups

***Figure 3.10**: Failure zones in beams*

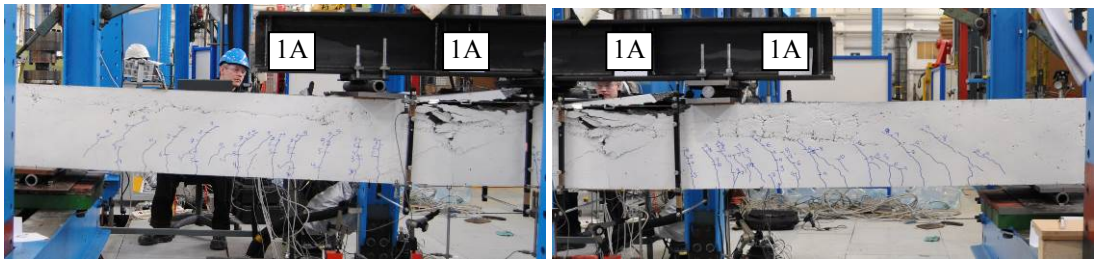

***Figure 3.11**: Beam 1A (only LWAC) at the end of testing. P = 116 kN, Δ = 40 mm*

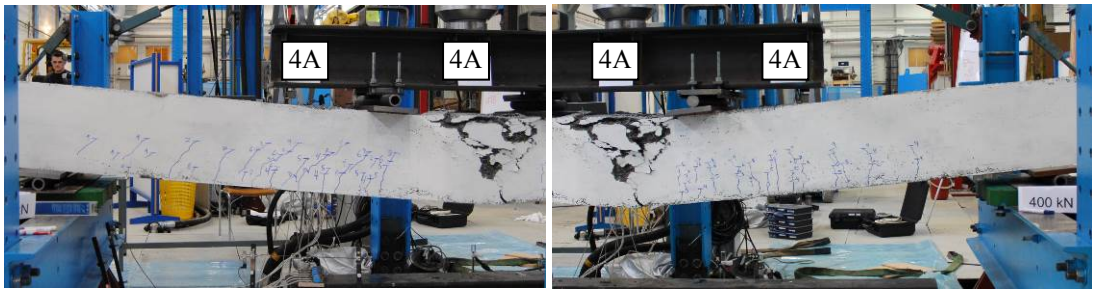

***Figure 3.12**: Beam 4A (fibre + stirrups) at the end of testing. P = 228 kN, Δ = 100 mm*

SINTEF Building and Infrastructure is the third largest building research institute in Europe. Our objective is to promote environmentally friendly, cost-effective products and solutions within the built environment. SINTEF Building and Infrastructure is Norway's leading provider of research-based knowledge to the construction sector. Through our activity in research and development, we have established a unique platform for disseminating knowledge throughout a large part of the construction industry.

COIN – Concrete Innovation Center is a Center for Research based Innovation (CRI) initiated by the Research Council of Norway. The vision of COIN is creation of more attractive concrete buildings and constructions. The primary goal is to fulfill this vision by bringing the development a major leap forward by long-term research in close alliances with the industry regarding advanced materials, efficient construction techniques and new design concepts combined with more environmentally friendly material production.